Energy Reports 7 (2021) 1798–1807

Contents lists available at ScienceDirect

Energy Reports

journal homepage: www.elsevier.com/locate/egyr

# Performance analysis of different arrangements of a new layout dish-Stirling system

Cheng Zhang [a], Qing Xu [a,*], Yanping Zhang [b], Inmaculada Arauzo [c], Chongzhe Zou [b]

[a] School of Mechanical and Power Engineering, Guangdong Ocean University, Zhanjiang 524008, China
[b] School of Energy and Power Engineering, Huazhong University of Science and Technology, Wuhan 430074, China
[c] CIRCE Research Institute, University of Zaragoza, Maria de Luna, Zaragoza 50009, Spain

ARTICLE INFO

*Article history:*
Received 28 August 2020
Received in revised form 10 January 2021
Accepted 1 March 2021
Available online 31 March 2021

*Keywords:*
Stirling cycle
Stirling engine model
Stirling engine array
Flow order

ABSTRACT

Cascade solar thermal systems provide a new direction for solar power generation. This paper focuses on the configuration optimization of a cascade solar system in which a Stirling engine array is applied. The array has multiple configurations. To find out the influence of the configuration on the performance of the engine array, five basic connection types were proposed. A Stirling engine model considering various losses and irreversibilities was developed. The model was evaluated by considering the prototype GPU-3 Stirling engine as a case study. Stirling engine array models were developed based on the Stirling engine model. Global efficiency and power of different connection types of Stirling engine arrays with the same hot and cold flows were evaluated. The effects of different factors on the performance of the Stirling engine arrays were considered. The result shows that flow order, the co-current flow or the counter-current flow, has little influence on the engine array performance. The maximum differences of thermal efficiency and output power of different flow orders are 0.39% and 0.70%, respectively. Serial flow connection type is the best for a Stirling engine array to obtain the best performance and adaptability for given heating and cooling fluids.



## 1. Introduction

With the emphasis on energy and environmental impact, solar energy, which has the advantages of wide distribution, a huge amount, inexhaustible and no pollution, has received much attention from many countries and been regarded as the best potential alternative for fossil energy. Concentrating solar thermal power generation is another form of power generation technology except for solar photovoltaic power generation. Compared to solar photovoltaic, solar thermal power is gaining more attention for its advantages as higher energy density, smooth power generation, good grid compatibility, easy to integrate with existing fossil power plants. There are three types of concentrating solar power (CSP) technologies being commercially applied: parabolic trough, parabolic dish and power tower. Amongst the three solar thermal power technologies, parabolic trough is the most mature and commercially deployed technology. However, it has a low concentration ratio, the receiver temperature is relatively low, the solar-to-electric efficiency is relatively low. Parabolic dish can obtain high-temperature thermal energy, its solar-to-electric efficiency is higher than parabolic trough. Besides, one advantage of parabolic dish is that it requires much less water for power generation. However, solar parabolic dish is not a large-scale application. It is mainly applied for distributed power generation for its compact structure and easy installation. Solar power tower has a very high concentration ratio when more heliostats are used, the receiver temperature can be very high and it can be applied for large-scale applications. However, it has some disadvantages such as high investment and high system complexity.

It is very important to find out a way to utilize the advantages of existing solar thermal power technologies and overcome their disadvantages. In other words, to find out a new technology with higher efficiency and lower cost is the key.

Great attention has focused on the application using a parabolic dish to collect heat. Some researchers investigated the impact of various parameters on the optical and thermal performance of the solar dish receivers using the Monte Carlo Ray Tracing Method (MCRTM) and/or numerical modeling method. Some researchers considered applications with different ways to use the collected heat. Loni et al. (2016) considered a system using a parabolic dish for an organic Rankine cycle. In the proposed system, the thermal oil is used as the working fluid to transport the collected heat for the organic Rankine cycle. Wang et al. (2014) proposed an inverse design method for a cavity receiver used in a solar dish Brayton system. Craig et al. (2016) evaluated a parabolic dish tubular receiver used in a dish Brayton cycle. An approach for incorporating a complex geometry like a tubular receiver

* Corresponding author.
*E-mail address:* hustquick@gdou.edu.cn (Q. Xu).

https://doi.org/10.1016/j.egyr.2021.03.003

**Nomenclature**

| | |
|---|---|
| $A$ | Heat transfer area, $m^2$ |
| $c_p$ | Heat capacity of Stirling engine working gas at constant pressure, J/(kg K) |
| $c_v$ | Heat capacity of Stirling engine working gas at constant volume, J/(kg K) |
| $e$ | Regenerator effectiveness |
| $f$ | Friction factor |
| $J$ | Annular gap cylinder displacer, m |
| $K$ | Dead volume factor, $m^3$/K |
| $m$ | Mass of working fluid in Stirling engine, kg |
| $n$ | Amount of gas, mol |
| $n_{se}$ | Number of Stirling engines in SEA |
| $p$ | Pressure, Pa |
| $P$ | Power, W |
| $Q$ | Absorbed heat, J |
| $q_m$ | Mass flow rate, kg/s |
| $Rg$ | Gas constant, J/(kg K) |
| $s_{se}$ | Speed of Stirling engine, $s^{-1}$ |
| $T_H$ | Highest temperature of expansion space, K |
| $T_L$ | Lowest temperature of compression space, K |
| $T_R$ | Regenerator temperature, K |
| $T_w$ | Wall temperature, K |
| $U$ | Overall heat transfer coefficient, W/($m^2$ K) |
| $V_C$ | Compression volume, $m^3$ |
| $V_D$ | Total dead volume, $m^3$ |
| $V_E$ | Expansion volume, $m^3$ |
| $V_{DC}$ | Cold space dead volume, $m^3$ |
| $V_{DH}$ | Hot space dead volume, $m^3$ |
| $V_{DR}$ | Regenerator dead volume, $m^3$ |
| $W$ | Output work, J |
| $Z$ | Displacer stroke, m |

**Abbreviations**

| | |
|---|---|
| SEA | Stirling Engine Array |

**Greek Symbols**

| | |
|---|---|
| $\gamma_H$ | Space ratio in process 12 |
| $\gamma_L$ | Space ratio in process 34 |
| $\gamma$ | Specific heat ratio ($c_p/c_v$) |
| $\theta$ | Crank angle, rad |
| $\mu$ | Dynamic viscosity, kg/(m s) |

**Subscripts**

| | |
|---|---|
| $c$ | Cooling fluid |
| $cw$ | Cooler wall |
| $h$ | Heating fluid |
| $hw$ | Heater wall |
| $i$ | Inlet |
| $o$ | Outlet |
| $p$ | Piston |
| $r$ | Regenerator |
| $th$ | Theoretical |

generated using CFD software into SolTrace was developed. Aichmayer et al. (2015) presented a hybrid solar micro gas-turbine system integrating volumetric solar dish receiver. Concerning the solar dish receiver integration, both pressurized and atmospheric configurations have been considered. Lovegrove et al. (2004) presented an idea of using a parabolic dish array to provide heat for ammonia-based thermochemical energy storage. Buscemi et al. (2020) presented a comprehensive mathematical model for a new type of solar air heater, and the experimental data show that the presented model is reliable.

A large number of studies have been done on Stirling engine analysis. To describe a Stirling engine behavior precisely is a difficult task due to the various losses and irreversibilities in the engine. Researchers have done a lot of work to build a precise Stirling engine model. Different models of Stirling engines were developed using empirical, analytical and numerical methods.

Among these methods, numerical methods provide the most accurate models. Urieli and Berchowitz (1984) proposed an adiabatic model of Stirling engine considering some irreversible effects such as non-ideal heat transfer processes and pressure drop effect using numerical methods. The model is known as the Simple model. Many researchers developed more accurate models based on the Simple model by using alternative methods or including more loss mechanisms. Ni et al. (2016) proposed an improved Simple analytical model that considers the influence mechanism of rotary speed, pressure and working gas in the view of heat/power losses for Stirling engine performance. Jia et al. (2016) developed a numerical model of a free-piston engine generator. The dynamic equations have been linearized to simplify the model to a one-degree forced vibration system with various damping. The solving time of the proposed fast response model can be significantly reduced compared to previous numerical models. Babaelahi and Sayyaadi (2014) proposed an alternative method to calculate the regeneration heat loss and pumping losses, which is more suitable for preliminary engine design and optimization, known as the Simple II model. Abbas (2014) considered the effects of non-ideal regeneration, shuttle loss and heat conduction losses based on the Simple model. Araoz et al. (2015) developed a rigorous Stirling engine model with adiabatic working spaces, isothermal heat exchangers. It considers dead volumes, and imperfect regeneration, mechanical pumping losses due to friction, limited heat transfer and thermal losses on the heat exchangers. The model is suitable for different engine configurations ($\alpha$, $\beta$ and $\gamma$ engines). Babaelahi and Sayyaadi (2015) proposed a new numerical thermal model based on polytropic expansion/compression processes. Differential equations in the expansion/compression processes were modified to polytropic processes in the new model. The new model shows a better performance prediction compared with previous models. Karabulut et al. (2019) used a modified Schmidt formula which takes into account the pressure differences between nodal volumes caused by flow friction. The optimum thermal efficiency and torque of the engine were determined under given conditions.

With the development of finite-time thermodynamics, many researchers studied the finite-time thermodynamic performance of the Stirling engine. This analysis can also be used in the case of irreversible machines further considering the internal irreversibilities of a Stirling engine such as friction, pressure drop and entropy generation (Barreto and Canhoto, 2017). Wu et al. (1998) developed a numerical model considering the finite-time effect to find out the relationship between the net power output and thermal efficiency of the engine. Yaqi et al. (2011) developed a mathematical model of a high-temperature differential dish-Stirling system with finite-time thermodynamics. Finite-rate heat transfer, regenerative heat losses, conductive thermal bridging losses and finite regeneration processes of the Stirling engine were considered in the model. Hosseinzade et al. (2015) presented a new closed-form thermal model for the thermal simulation of Stirling engines based on the combination of polytropic analysis of expansion/compression processes and the concept of finite speed

thermodynamics. Instead of the finite-time method, Ahmadi et al. (2016b) proposed a finite-speed thermodynamic analysis based on the first law of thermodynamics for a closed system with finite speed and the direct method. The effects of heat source temperature, regenerating effectiveness, volumetric ratio, piston stroke as well as rotational speed are included in the analysis. Chen et al. (2007) developed a heat-engine cycle model using finite-time thermodynamics. The model considered the losses due to heat-resistance, heat leaks and internal irreversibility, which is applicable for generalized irreversible universal steady-flow heat-engine cycles.

On the other side of the researches, multi-objective optimization algorithms were used considering multi-variables to obtain a better performance were paid for attention by numbers of researchers recently. Ahmadi et al. (2016a) performed the thermodynamic analysis of a solar dish Stirling engine based on finite-time thermodynamics. Then the NSGA-II algorithm was applied. Three objectives, thermal efficiency, entransy loss rate, and power output, were set as the objectives and three well-known decision-making methods have been employed in the algorithm. Li et al. (2016) developed a multi-objective optimization model of a solar energy powered gamma type Stirling engine using Finite Physical Dimensions Thermodynamics (FPDT) method by multi-objective criteria. A genetic algorithm was used to get the Pareto frontier, and optimum points were obtained using the decision different making methods. Results show that total thermal conductance, hot temperature, stroke and diameter ratios can be improved. Patel and Savsani (2016) developed a strategy for multi-objective optimization for Stirling engines using TS-TLBO (tutorial training and self-learning inspired teaching–learning-based optimization) algorithm. An application example with eleven decision variables and three objectives are considered. Luo et al. (2016) proposed a multiple-objective optimization method that combines multiple optimization algorithms including differential evolution, genetic algorithm, and adaptive simulated annealing. The optimization considers five decision variables, including engine frequency, mean effective pressure, the temperature of heating source, number of wires in the regenerator matrix, and the wire diameter of the regenerator for maximum efficiency and output power.

However, dish-Stirling system has not received wide commercial deployment yet. It is a solar-only generation system, without storage or simple hybridization. Compared with photovoltaics, which is also a solar-only generation system, dish Stirling could not compete in terms of reliability nor cost per unit of energy produced. The Stirling engine capacity is mainly constrained by two factors: dish collector size and Stirling engine size. The dish size is limited for the cost and difficulty of production of large mirrors. The Stirling engine size is limited for its low power-to-weight ratio. The tracking feature of dish collector limits the weight of the engine on the focal point. Besides, the size of the engine is limited for it overlaps part of the collector.

This paper presents a new layout scheme of dish-Stirling system demonstrated in Fig. 1. In the new scheme, Stirling engines are put on the ground as a Stirling engine array (SEA). Heat collected by multiple dish collectors is supplied to the SEA by heating fluid. The new scheme has some advantages. Due to the heat transfer fluid, a heat storage system becomes feasible. Heat provided to the SEA may be provided by other types of collectors, a combination of different types of collectors, or different kinds of heat sources. On the other hand, since the engines are static installations on the ground where space and weight are not at a premium anymore, they can reach higher capacities.

In the proposed scheme, Stirling engines can be connected in different connection types, and their performance is relative with their connection types according to their arrangement. However,

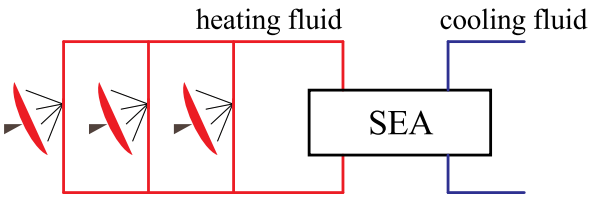


**Fig. 1.** New layout scheme of a dish-Stirling system.

the literature review indicates that the analysis of arrangements of Stirling engines, classification and performance of the SEA, has not yet been reported. In this regard, this paper investigated the connection types of SEA and its influence on SEA performance. According to Organ's theory (Organ, 1997), one equivalent analytical Stirling engine model always exists for different types ($\alpha$ type, $\beta$ type and $\gamma$ type) of engines. To find out the influence of the connection type of SEA and to avoid falling into the problem of developing a specific Stirling engine model, a $\beta$ type Stirling engine model based on some assumptions and simplifications was developed. This model was evaluated using experimental data of the General Motor GPU-3 Stirling engine prototype. Imperfect regeneration and some irreversibilities were considered. Heat transfer analysis of the Stirling engine with heating and cooling fluids was also included. SEA models of different connection types were built depending on the engine model. The impacts of different parameters on the performance of these models were analyzed.

## 2. Connection types of SEA

For a single Stirling engine, the heat transfer processes between fluids and engine are independent and irrelevant with the direction of the flows, which means the efficiency and power are not affected by the direction of fluids. However, for an SEA, the connection type will affect the temperature profiles through the array and the specific work production, both of which will determine the efficiency and power of the SEA. It is practically significant to investigate the influence of the connection type of an SEA on its performance. Using parallel flow, on the one hand, will reduce the flow rate of the fluid, which will reduce the power of each engine; however, on the other hand, will take the advantage of higher inlet heating fluid temperature (or lower inlet cooling fluid temperature), which may increase the power of each engine. Using serial flow, on the one hand, will increase the flow rate of the fluid, which will increase the power of each engine; however, on the other hand, the inlet heating fluid temperature reduces with the flow direction (or the inlet cooling fluid temperature increases with the flow direction), which leads to lower engine power and efficiency because of reduced $T_{max}$ of the cycle along the flow direction. Using the same order will lead to largest fluid temperature difference (temperature difference of the heating and cooling fluids) at the upstream engines and smallest fluid temperature difference at the downstream engines. Using the reverse order will lead to higher averaged fluid temperature differences in the engines. For a heat exchanger, the reverse order (counterflow), which leads to a smaller fluid temperature difference, has a better heat transfer effect for its lower exergy loss. However, for a Stirling engine, the smaller fluid temperature difference leads to lower performance due to the lower temperature difference of the working gas in the hot space and cold space. To find out the influence of the connection types on the performance of an SEA, it is essential to classify the connection types.

Five basic connection types of SEA were summarized according to the direction-irrelevant feature of Stirling engine, as shown

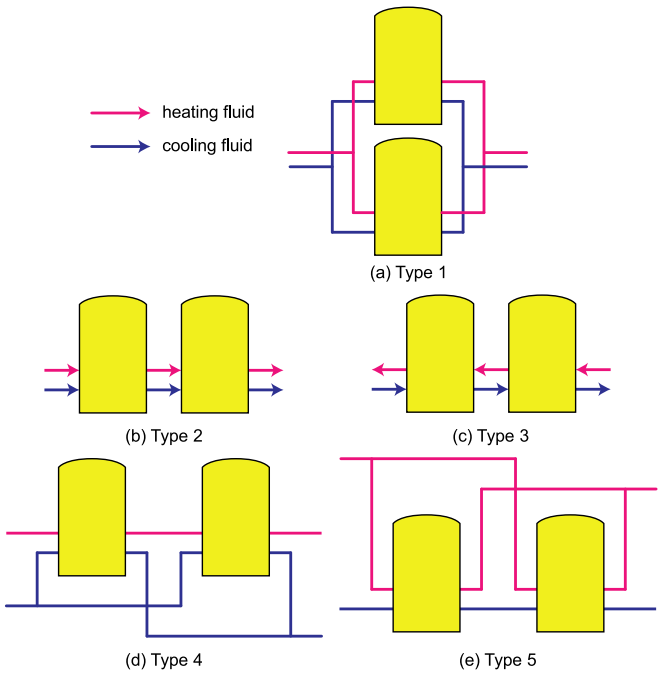


**Fig. 2.** Five basic connection types of SEA.

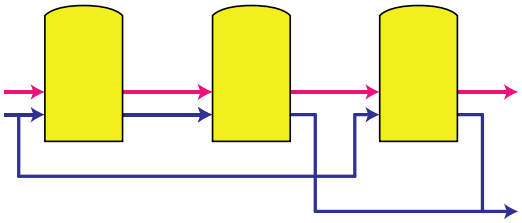

**Fig. 3.** An instance of connection type of an SEA.

in Fig. 2. Type 1 is parallel flow, Type 2 is co-current serial flow, Type 3 is counter-current serial flow, Type 4 is heating fluid in serial flow and cooling fluid in parallel flow and Type 5 is heating fluid in parallel flow and cooling fluid in serial flow. All other connection types are the combination of these five basic connection types. For instance, an SEA described in Fig. 3 is a combination of Type 2 and Type 4.

## 3. Thermodynamic analysis of Stirling engine

### 3.1. Stirling engine model

#### 3.1.1. Theoretical Stirling cycle

In a Stirling cycle, there are two isothermal processes that exchange heat with heating and cooling fluids, two isochoric processes that exchange heat with the regenerator. Fig. 4 shows the schematic of a Stirling cycle, process 1-2 and process 3-4 are the two isothermal processes, process 2-3 and process 4-1 are the two isochoric processes. The heat absorbed by regenerator in process 4-1 is reused in process 2-3, but only able to heat the working gas from 2 to 3' due to the imperfect regeneration. $e$ is defined as the regenerator effectiveness for the imperfect regeneration (Formosa and Despesse, 2010):

$$e = \frac{T_R - T\_L}{T_H - T_L} \tag{1}$$

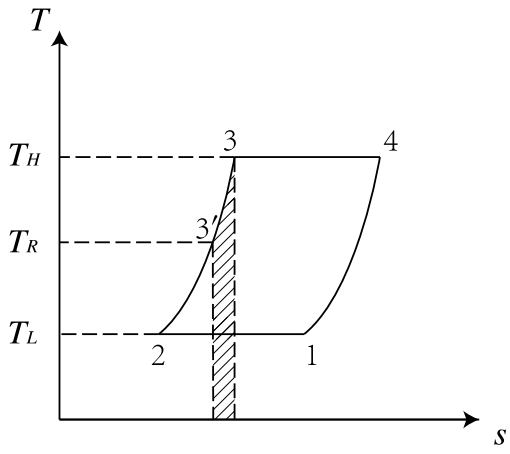


**Fig. 4.** $T$-$s$ diagram of a Stirling cycle.

where $T_H$ is the temperature in the hot space, $T_L$ is the temperature in the cold space, $T_R$ is the effective working fluid temperature in the regenerator.

In order to obtain a simplified analytical model, several simplifications were made:

- The working gas in Stirling engines is ideal gas.
- No heat leakage to the environment for Stirling engines.
- Overall heat transfer coefficients of the fluids are constant.
- The engine is working with adiabatic compression and expansion spaces.
- A linear temperature distribution regenerator behavior is assumed (Formosa and Despesse, 2010) so that the effective working fluid temperature can be obtained by

$$T_R = \frac{T_H - T_L}{\ln(T_H - T_L)} \tag{2}$$

To consider internal irreversibilities in the Stirling cycle made by dead volumes, as described in Duan et al. (2014), total dead volume $V_D$ is divided into heater dead volume $V_{DH}$, regenerator dead volume $V_{DR}$ and cooler dead volume $V_{DC}$. There exists a factor $K$ to describe the dead volumes under different temperatures. $K$ is relevant to temperatures in the process and regenerator effectiveness.

$$K = \frac{V_{DH}}{T_H} + \frac{V_{DR}}{T_R} + \frac{V_{DC}}{T_L} \tag{3}$$

For the isothermal compression process 1-2, the output work

$$W_{12} = \int_{V_E+V_C}^{V_E} p_{12}\mathrm{d}V = -mRT_L \ln \frac{V_E + V_C + KT_L}{V_E + KT_L} \tag{4}$$

For the isothermal expansion process 3-4, the output work

$$W_{34} = \int_{V_E}^{V_E+V_C} p_{34}\mathrm{d}V = -mRT_H \ln \frac{V_E + V_C + KT_H}{V_E + KT_H} \tag{5}$$

Defining $\gamma_H = (V_E + V_c + KT_H)/(V_E + KT_H)$ and $\gamma_L = (V_E + V_c + KT_L)/(V_E + KT_L)$, so in a cycle, the theoretical output work

$$W_{th} = W_{12} + W_{34} = mR\,(T_H \ln \gamma_H - T_L \ln \gamma_L) \tag{6}$$

For the isochoric heating process 3'-3, the absorbed heat

$$Q_{3'3} = nc_v\,(T_H - T_R) = \frac{nR}{\gamma - 1}\,(T_H - T_L) = \frac{mR_g}{\gamma - 1}(1 - e)\,(T_H - T_L)$$
$$= \frac{1 - e}{\gamma - 1} mR_g (T_H - T_L) \tag{7}$$

For the isothermal expansion process 3-4, the absorbed heat

$$Q_{34} = W_{34} = mR_g T_H \ln \gamma_H \tag{8}$$

In a cycle, the theoretical absorbed heat

$$Q_{th} = Q_{3'3} + Q_{34} = \frac{1-e}{\gamma - 1} mR_g (T_H - T_L) + mR_g \mathrm{T_H} \ln \gamma_H \tag{9}$$

*3.1.2. Irreversibilities and losses*

a. Non-ideal heat transfer effect
Because of the non-ideal heater and cooler, the working fluid temperature ($T_H$, $T_L$) in these two heat exchangers is less/higher than the wall temperature ($T_{hw}$, $T_{cw}$), respectively. $T_H$ and $T_L$ can be corrected by the wall temperatures as follows:

$$T_H = T_{hw} - \frac{Qs_{se}}{h_h A_{hw}} \tag{10}$$

$$T_L = T_{cw} - \frac{(Q-W)s_{se}}{h_c A_{cw}} \tag{11}$$

The heat transfer coefficient can be obtained using the following correlation (Babaelahi and Sayyaadi, 2015):

$$h_{h,c} = \frac{\mu c_p f_{Re}}{2D_{h,c} Pr_{h,c}} \tag{12}$$

where $f_{Re}$ is a Reynolds friction factor defined as (Babaelahi and Sayyaadi, 2015):

$$f_{Re} = 0.0791 Re_{h,c}^{0.75} \tag{13}$$

$Re_{h,c}$, $Pr_{h,c}$ and $D_{h,c}$ are Reynolds number, Prandtl number and hydraulic diameter of the heater/cooler exchanger, where $Re_{h,c} > 4000$.

b. Effect of pressure drop
Pressure drops in the heat exchangers cause power losses of the Stirling engine. The pressure drops can be obtained by (Urieli and Berchowitz, 1984):

$$\Delta_p = -\frac{2 f_{Re} \mu u V}{d^2 A} \tag{14}$$

where $u$ is the working gas speed, $V$ is volume, $A$ is flow cross-section area.
The net power loss of the Stirling engine due to pressure drop of the heat exchangers can be evaluated by:

$$W_{pd} = \oint \sum_{i=E,C} (\Delta p_i \frac{\mathrm{d}V_i}{\mathrm{d}\theta}) \mathrm{d}\theta \tag{15}$$

c. Effect of finite speed of piston and mechanical friction
Due to the finite speed of piston, the pressure on the piston surface is different from the pressure of expansion and compression spaces. It has been demonstrated that the pressure on the piston surface in the expansion process is less than the mean pressure in the expansion space. Similarly, the pressure on the piston surface in the compression process is greater than the mean pressure in the compression space. This means the output work is less than the theoretical value. Besides, the output work also reduces due to mechanical friction. The output work loss due to finite speed of piston and mechanical friction can be obtained as follows (Babaelahi and Sayyaadi, 2015):

$$W_{fs} = \oint p(\frac{a u_p}{c} + \frac{\Delta_{p_f}}{p}) \mathrm{d}V \tag{16}$$

$p$ is the mean pressure in the compression/expansion space, $u_p$ is the velocity of the piston, $c$ is the average speed of molecules and $\Delta p_f$ is the pressure loss due to mechanical friction. $\Delta p_f$, $a$ and $c$ can be obtained by (Heywood, 1988):

$$\Delta p_f = 0.97 + 0.009 s_{se} \tag{17}$$

$$\mathrm{a} = \sqrt{3\gamma} \tag{18}$$

$$\mathrm{c} = \sqrt{3R_g T} \tag{19}$$

Where $s_{se}$ is the speed of the engine, Hz.

d. Energy losses due to internal conduction
The temperature differs from the heater and cooler, heat losses from the heater to cooler exists due to internal conduction through the walls of the regenerator (Babaelahi and Sayyaadi, 2014). The internal conduction loss in a cycle can be obtained by:

$$Q_{id} = \frac{k_r A_r}{L_r s_{se}} (T_{hw} - T_{cw}) \tag{20}$$

where, $k_r$, $A_r$ and $L_r$ denote the regenerator matrix conductivity, regenerator conductive area, and regenerator length respectively.

e. Energy losses due to shuttle conduction
The displacer shuttles between the expansion and compression space. It absorbs heat during the hot end of its stroke and releases it during the cold end of its stroke. This heat loss can be estimated as (Timoumi et al., 2008):

$$Q_{sc} = 0.4 \frac{Z^2 k_p D_p}{J L_d s_{se}} (T_H - T_L) \tag{21}$$

where, $Z$, $k_p$, $D_p$, $J$ and $L_d$ denote the displacer stroke, piston thermal conductivity, displacer diameter, gap between the displacer and the cylinder, and length of the displacer respectively.

So, in a Stirling engine, the total absorbed heat in a cycle

$$Q = Q_{th} + Q_{id} + Q_{sc} \tag{22}$$

the output work

$$W = W_{th} - W_{pd} - W_{fs} \tag{23}$$

Power of the Stirling engine

$$P = W s_{se} \tag{24}$$

Efficiency of the Stirling engine

$$\eta = W/Q \tag{25}$$

*3.2. Model validation*

The evaluation of the thermal model developed was performed by considering the GPU-3 Stirling engine as a case study. The design specifications of the GPU-3 Stirling engine are indicated in Table 1. The thermal efficiency and output power of the proposed Stirling engine model were compared with previous thermal models and experimental data as shown in Tables 2 and 3.

It can be found that the proposed model has much better agreement with the experimental results than previous thermal models at various rotation speeds and mean effective pressures. It is required to mention that in all thermal models both power $W$ and input heat $Q$ were determined by the thermal process of heat transfer between the wall and working gas. In the proposed model, $W$ and $Q$ are obtained by Eqs. (10) and (11). Therefore, all three parameters $W$, $Q$ and $\eta$ are determined by the thermal model and input parameters to the model. These input parameters include heater, cooler, mean effective pressure, type of working gas and geometrical specification of the engine.

**Table 1**
Design specifications of the GPU-3 Stirling engine (Babaelahi and Sayyaadi, 2015; Martini, 1983).

| Parameter | Value | Parameter | Value |
|---|---|---|---|
| working gas | helium | mass of the working gas | 1.136 g |
| **heater** | | | |
| number of tubes | 40 | | |
| tube external diameter | 4.83 mm | tube internal diameter | 3.02 mm |
| tube length (cylinder side) | 0.1164 m | tube length (regenerator side) | 0.1289 m |
| **cooler** | | | |
| number of tubes | 312 | tube external diameter | 1.59 mm |
| tube internal diameter | 1.09 mm | average tube length | 46.1 mm |
| **regenerator** | | | |
| number of regenerators | 8 | regenerator internal diameter | 22.6 mm |
| regenerator length | 22.6 mm | diameter of regenerator tube | 0.04 mm |
| material | stainless steel | | |
| **volume** | | | |
| swept vol. (expansion/compression) | 120.82/114.13 $cm^3$ | clearance vol. (expansion/compression) | 30.52/28.68 $cm^3$ |
| dead vol. (heater/cooler/regenerator) | 70.28/13.18/50.55 $cm^3$ | | |

**Table 2**
Thermal efficiency of previous thermal models, the proposed model and experimental data (at $T_{hw} = 922$ K and $T_{cw} = 288$ K).

| Rotation speed (Hz) | Mean effective pressure (MPa) | Thermal efficiency predicted by the simple analysis (variable Pr (Urieli and Berchowitz, 1984)) | | | Thermal efficiency predicted by the adiabatic analysis (simple II (Babaelahi and Sayyaadi, 2014)) | | | Thermal efficiency predicted by the proposed Stirling engine model | | | Experimental efficiency (Babaelahi and Sayyaadi, 2015) |
|---|---|---|---|---|---|---|---|---|---|---|---|
| | | Value (%) | Error (%) | Average error (%) | Value (%) | Error (%) | Average error (%) | Value (%) | Error (%) | Average error (%) | Actual value (%) |
| 16.67 | 2.76 | 38.72 | 18.22 | 17.90 | 32.48 | 11.98 | 12.85 | 28.16 | 7.66 | 12.10 | 20.50 |
| 25.00 | | 36.16 | 15.46 | | 31.21 | 10.51 | | 27.75 | 7.05 | | 20.70 |
| 33.33 | | 33.79 | 15.79 | | 29.45 | 11.45 | | 27.43 | 9.43 | | 18.00 |
| 41.67 | | 31.48 | 16.28 | | 27.45 | 12.25 | | 27.17 | 11.97 | | 15.20 |
| 50.00 | | 29.12 | 17.32 | | 25.21 | 13.41 | | 26.94 | 15.14 | | 11.80 |
| 58.33 | | 29.74 | 24.34 | | 22.89 | 17.49 | | 26.74 | 21.34 | | 5.40 |
| 25.00 | 4.14 | 35.65 | 10.85 | 11.46 | 32.29 | 7.49 | 8.28 | 27.29 | 2.49 | 6.65 | 24.80 |
| 33.33 | | 33.52 | 9.62 | | 30.40 | 6.50 | | 26.94 | 3.04 | | 23.90 |
| 41.67 | | 31.48 | 10.18 | | 28.39 | 7.09 | | 26.65 | 5.35 | | 21.30 |
| 50.00 | | 29.45 | 11.25 | | 26.33 | 8.13 | | 26.39 | 8.19 | | 18.20 |
| 58.33 | | 27.40 | 15.40 | | 24.21 | 12.21 | | 26.17 | 14.17 | | 12.00 |
| 41.67 | 5.52 | 31.20 | 8.70 | 10.82 | 28.59 | 6.09 | 8.11 | 26.24 | 3.74 | 7.48 | 22.50 |
| 50.00 | | 29.33 | 10.53 | | 26.62 | 7.82 | | 25.97 | 7.17 | | 18.80 |
| 58.33 | | 27.44 | 13.24 | | 24.62 | 10.42 | | 25.73 | 11.53 | | 14.20 |
| 50.00 | 6.90 | 29.07 | 10.37 | 11.73 | 26.61 | 7.91 | 9.19 | 25.62 | 6.92 | 9.05 | 18.70 |
| 58.33 | | 27.29 | 13.09 | | 24.67 | 10.47 | | 25.37 | 11.17 | | 14.20 |

Tables 2 and 3 indicate that when the mean effective pressure of the engine increases from 2.76 MPa to 6.90 MPa, the best performance (efficiency and power) prediction of the proposed model exists. When rotation speed increases from 16.67 Hz to 58.33 Hz, error in prediction of the performance of the proposed model increases. The proposed model may have the best performance prediction at a low rotation speed, with mean effective pressure between 4.14 MPa and 5.52 MPa.

The proposed model improved errors ($s_{se} = 25$ Hz, $p = 4.14$ MPa) on the thermal efficiency and output power and reduced these errors from 7.49% and 110.11% (as difference) obtained in simple II model (Babaelahi and Sayyaadi, 2014) to 2.49% and 1.56% (as difference), respectively. However, there is still some discrepancy between the simulation results of the proposed model and the experimental data. This may be due to some existing experimental irreversibilities that are not considered in the proposed model. In future researches, more accurate models of the Stirling engine may be developed by considering those existing irreversibilities such as heat leakage to the environment, gas spring hysteresis and non-adiabatic compression and expansion spaces. It is worth pointing that there are more accurate Stirling engine models. For example, polytropic simulation models of the Stirling engine shows higher accuracy than our proposed model (Babaelahi and Sayyaadi, 2015; Hosseinzade et al., 2015). However, the model needs more costly calculations and the polytropic indexes are engine-specific.

### 3.3. Heat transfer between the engine and the fluids

For a Stirling engine thermal process, the wall temperatures of the heater and cooler are considered to be uniform and constant. The heat transferred between the wall and the fluids is

$$(T_w - T)\, U \mathrm{d}A = q_m c_p \mathrm{d}T \tag{26}$$

with $T(0) = T_i$, $T(A) = T_o$,

$$\frac{T_o - T_w}{T_i - T_w} = \exp\left(-\frac{UA}{q_m c_p}\right) \tag{27}$$

For a Stirling engine, $T_{hw}$ or $T_{cw}$ can be used to substitute $T_w$ to get the relationships between $T_{i,h}$, $T_{o,h}$ and $T_{hw}$, or $T_{i,c}$, $T_{o,c}$ and $T_{cw}$ respectively.

$$\frac{T_{o,h} - T_{hw}}{T_{i,h} - T_{hw}} = \exp\left(-\frac{U_h A_h}{q_{m,h} c_{p,h}}\right) \tag{28}$$

**Table 3**
Output power of previous thermal models, the proposed model and experimental data (at $T_{hw} = 922$ K and $T_{cw} = 288$ K).

| Rotation speed (Hz) | Mean effective pressure (MPa) | Output power predicted by the simple analysis (variable Pr (Urieli and Berchowitz, 1984)) | | | Output power predicted by the adiabatic analysis (simple II (Babaelahi and Sayyaadi, 2014)) | | | Output power predicted by the proposed Stirling engine model | | | Experimental output power (Babaelahi and Sayyaadi, 2015) |
|---|---|---|---|---|---|---|---|---|---|---|---|
| | | Value (kW) | Error (%) | Average error (%) | Value (kW) | Error (%) | Average error (%) | Value (kW) | Error (%) | Average error (%) | Actual value (kW) |
| 16.67 | 2.76 | 1.796 | 119.02 | 272.03 | 1.772 | 116.10 | 254.71 | 0.861 | 4.98 | 104.84 | 0.82 |
| 25.00 | | 2.555 | 128.13 | | 2.500 | 123.12 | | 1.253 | 11.88 | | 1.12 |
| 33.33 | | 3.215 | 165.70 | | 3.117 | 157.60 | | 1.632 | 34.88 | | 1.21 |
| 41.67 | | 3.769 | 211.49 | | 3.615 | 198.76 | | 2.001 | 65.37 | | 1.21 |
| 50.00 | | 4.195 | 303.37 | | 3.973 | 282.08 | | 2.362 | 127.12 | | 1.04 |
| 58.33 | | 4.505 | 704.46 | | 4.203 | 650.54 | | 2.715 | 384.82 | | 0.56 |
| 25.00 | 4.14 | 3.844 | 114.75 | 259.70 | 3.761 | 110.11 | 158.41 | 1.818 | 1.56 | 39.83 | 1.79 |
| 33.33 | | 4.856 | 120.73 | | 4.708 | 114.00 | | 2.362 | 7.36 | | 2.20 |
| 41.67 | | 5.734 | 136.94 | | 5.501 | 127.31 | | 2.890 | 19.42 | | 2.42 |
| 50.00 | | 6.462 | 174.98 | | 6.126 | 160.68 | | 3.405 | 44.89 | | 2.35 |
| 58.33 | | 7.030 | 306.36 | | 6.573 | 279.94 | | 3.908 | 125.90 | | 1.73 |
| 41.67 | 5.52 | 7.645 | 133.08 | 180.02 | 7.334 | 123.60 | 164.91 | 3.742 | 14.09 | 43.68 | 3.28 |
| 50.00 | | 8.655 | 163.87 | | 8.206 | 150.18 | | 4.401 | 34.18 | | 3.28 |
| 58.33 | | 9.470 | 243.12 | | 8.858 | 220.94 | | 5.045 | 82.79 | | 2.76 |
| 50.00 | 6.90 | 10.79 | 140.50 | 287.04 | 10.22 | 160.13 | 263.63 | 5.362 | 36.44 | 97.75 | 3.93 |
| 58.33 | | 11.84 | 399.58 | | 11.07 | 367.13 | | 6.140 | 159.07 | | 2.37 |

$$\frac{T_{o,c} - T_{cw}}{T_{i,c} - T_{cw}} = \exp(-\frac{U_c A_c}{q_{m,c} c_{p,c}}) \tag{29}$$

Heat transferred from heating fluid to Stirling engine in a cycle

$$q_{m,h} c_{p,h} (T_{i,h} - T_{o,h})/s_{se} = Q \tag{30}$$

Heat transferred from Stirling engine to cooling fluid in a cycle

$$q_{m,c} c_{p,c} (T_{o,c} - T_{i,c})/s_{se} = Q - W \tag{31}$$

## 4. Modeling of the SEAs

As mentioned in Section 2, there are five basic connection types for an SEA. All other connection types are the combination of these five basic connection types. This paper investigates the five basic connection types.

To determine the performance of an SEA, models of all the Stirling engines need to be built depending on their thermodynamic characteristics. Stirling engines are chosen to have the same parameters including the same speed $s_{se}$. This is a reasonable assumption when using SEA for power generation, where the output power frequency should be constant. The speed of the Stirling engine can be calibrated by a speed controller system (Hooshang et al., 2016). To eliminate the interference of other factors, heating and cooling fluids are chosen to have the same parameters for different connection types of SEAs. To clearly find out the performance differences of different SEAs, large temperature differences of the heating/cooling fluids after heat exchange with the engines are preferred. Air was chosen as the cooling fluid instead of commonly used water to avoid small temperature rise and evaporation in the cooling process. The design parameters of Stirling engines are the same as shown in Table 4. Other parameters of Stirling engines and heating/cooling fluids in SEAs are shown in Table 1. The rotation speeds of the engines and mean effective pressures are chosen to be 25 Hz and 5 MPa respectively to get the best Stirling engine model for performance prediction, as pointed in Section 3.2.

In an SEA, there are 2 flows as shown in Fig. 2. In a serial flow, each engine's mass flow rate is $q_m$, and from the flow's direction, for $2 \le x \le n_{se}$, $T_{i,x} = T_{o,x-1}$. In a parallel flow, each engine's mass flow is $q_m/n_{se}$, for $2 \le x \le n_{se}$, $T_{i,x} = T_{i,h}$.

MATLAB was used as the programming tool to build the model of SEAs, and CoolProp was used to provide fluid properties for the MATLAB program. Five basic SEA models composed of the aforementioned Stirling engines and fluids were built. To compare SEA connection types under various conditions, several parameters are investigated to find out their effects on SEA performance.

**Table 4**
Parameters of SEA models.

| Parameter heating fluid | Value air | Parameter cooling fluid | Value air | Parameter | Value |
|---|---|---|---|---|---|
| $n_{se}$ | 6 | $s_{se}$ | 25 Hz | $p_{se}$ | $5 \times 10^6$ Pa |
| $U_h A_h$ | 180 W/K | $U_c A_c$ | 180 W/K | | |
| $q_{m,h}$ | 0.4 kg/s | $T_{i,h}$ | 1000 K | $p_{i,h}$ | $5 \times 10^5$ Pa |
| $q_{m,c}$ | 0.4 kg/s | $T_{i,c}$ | 300 K | $p_{i,c}$ | $5 \times 10^5$ Pa |

**Table 5**
Results of SEA models under specified parameters.

| Parameter | Value | Parameter | Value |
|---|---|---|---|
| $\eta_1$ | 0.2215 | $P_1$ | 8022 W |
| $\eta_2$ | 0.2273 | $P_2$ | 8483 W |
| $\eta_3$ | 0.2277 | $P_3$ | 8512 W |
| $\eta_4$ | 0.2227 | $P_4$ | 8116 W |
| $\eta_5$ | 0.2263 | $P_5$ | 8399 W |

## 5. Result analysis

SEA models with specified parameters in Table 4 were built and calculated. Results of the performances of the SEAs are shown in Table 5, it can be found that under specified parameters Type 3 has the highest efficiency and output power, while Type 1 has the lowest efficiency and output power.

### 5.1. Effects of $T_{i,h}$

According to the Carnot cycle efficiency formula, the temperature of the heating fluid determines the efficiency of the Stirling

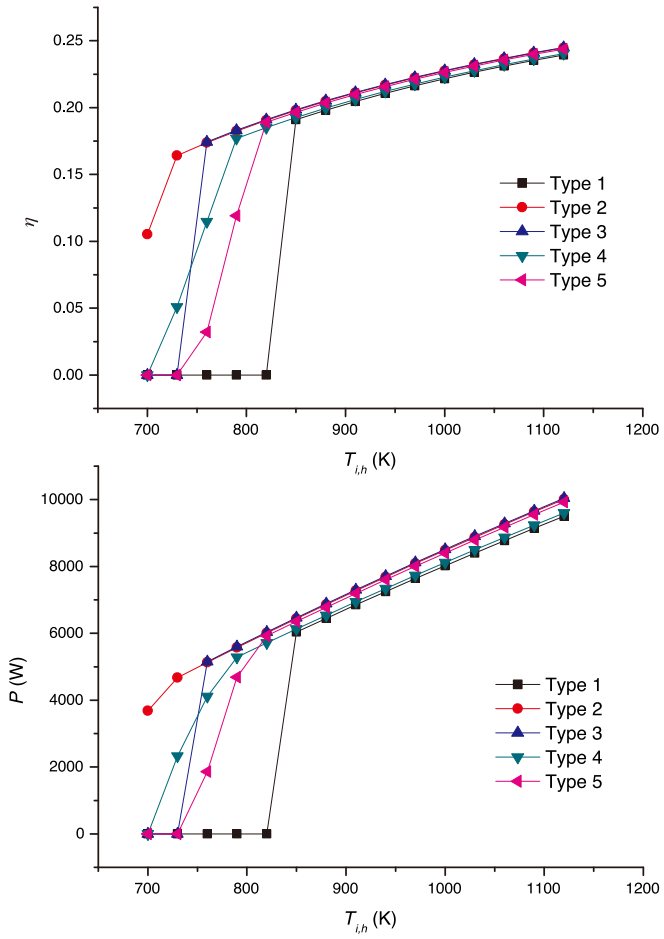


**Fig. 5.** Influence of $T_{i,h}$ on efficiency and power of SEA.

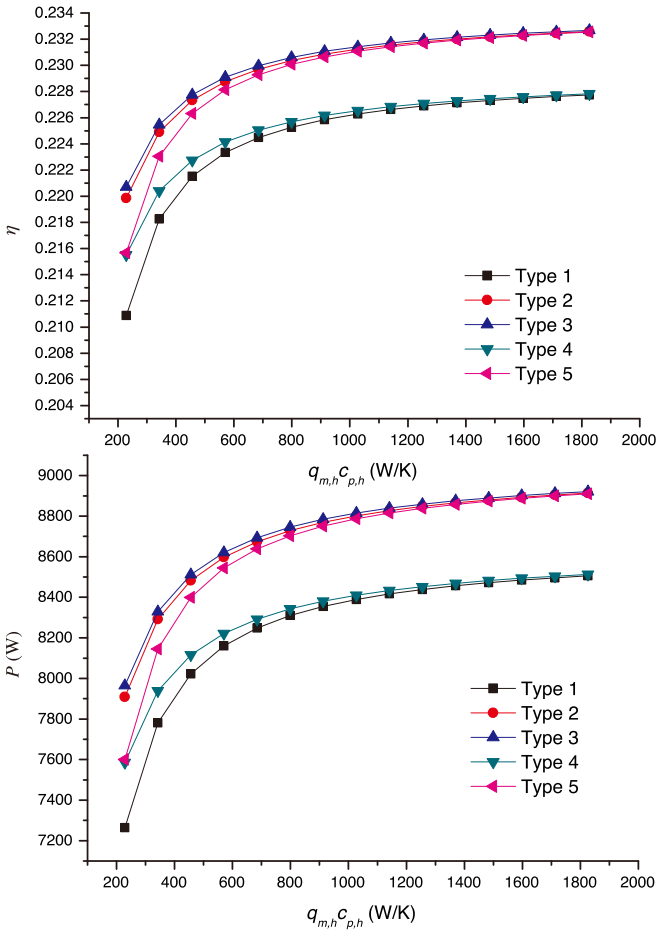


**Fig. 6.** Influence of $q_{m,h}c_{p,h}$ on efficiency and power of SEA.

engine array. For a Stirling engine, lower temperature heating fluid leads to lower efficiency. The efficiency and output power may drop to 0 due to its insufficient heating fluid temperature to drive the engine.

Curves of performance of SEAs and $T_{i,h}$ are shown in Fig. 5. As it is shown, with the increase of $T_{i,h}$, both $\eta$ and $P$ increase for all SEAs. For some types of SEA, when $T_{i,h}$ is lower than a critical temperature, some of the engines in the SEA will not work and there will be turning points on the $\eta$-$T_{i,h}$, $P$-$T_{i,h}$ curves. For example, in SEA of Type 1, when $T_{i,h}$ is lower than 820 K, all the engines stop working, turning points at 820 K can be found on the $\eta$-$T_{i,h}$, $P$-$T_{i,h}$ curves in Fig. 5. By checking the calculation results, it can be found that all the stopped engines have the same $T_H$ and $T_L$. The temperature differences of heat and cold fluids for the engines are not enough to drive the engines.

From curves in Fig. 5, it can be concluded that Type 2 and Type 3 have the best performance, and Type 2 has the best adaptability for lower $T_{i,h}$. All engines in Type 2 work when $T_{i,h}$ is 730 K. It can be interpreted that, in order for all engines in a parallel flow connection (Type 1, Type 4 and Type 5) to work, $T_{i,h}$ must be higher due to the lower $q_m$.

The flow order, co-current flow or counter-current flow, has little influence on the engine array performance. When all engines work, the difference of thermal efficiency of the SEA with Type 2 and Type 3 is from 0.15% to 0.33%; the difference of output power of the SEA with Type 2 and Type 3 is from 0.31% to 0.51%.

### 5.2. Effects of $q_m c_p$

According to Eqs. (30), (31), $q_m c_p$ (both $q_{m,h}c_{p,h}$ and $q_{m,c}c_{p,c}$) will affect the heat transfer process, which is one of the vital factors for the performance of SEA.

Curves of performance of SEAs and $q_{m,h}c_{p,h}$ are shown in Fig. 6. For a large $q_{m,h}c_{p,h}$ (> 800 W/K), Type 2, Type 3 and Type 5 have similar performance, which can be interpreted as the cooling fluid has the same properties for the two types of SEAs, and for a large $q_{m,h}c_{p,h}$, the heating fluid has similar effect after diverged. Similar performance of Type 1 and Type 4 can be also interpreted for the same reason.

The flow order, co-current flow or counter-current flow, has little influence on the engine array performance. The difference of thermal efficiency of the SEA with Type 2 and Type 3 is from 0.05% to 0.35%; the difference of output power of the SEA with Type 2 and Type 3 is from 0.10% to 0.62%.

Curves of performance of SEAs and $q_{m,c}c_{p,c}$ are shown in Fig. 7. For a connection type of SEA, the performance improves with the increase of $q_{m,c}c_{p,c}$. For a large $q_{m,c}c_{p,c}$ (> 800 W/K), Type 2 and Type 3 have similar performance, which means the flow order does not affect the performance of SEA with a large $q_{m,c}c_{p,c}$. There exists an intersection point (at 830 W/K) of curves of Type 4 and Type 5. For a larger $q_{m,c}c_{p,c}$, Type 4 has better performance and vice versa. This can be interpreted that larger $q_{m,c}c_{p,c}$ weaken the drawback of larger temperature rise of parallel flow, while for the heating fluid, a temperature drop in serial flow is smaller than in parallel flow.

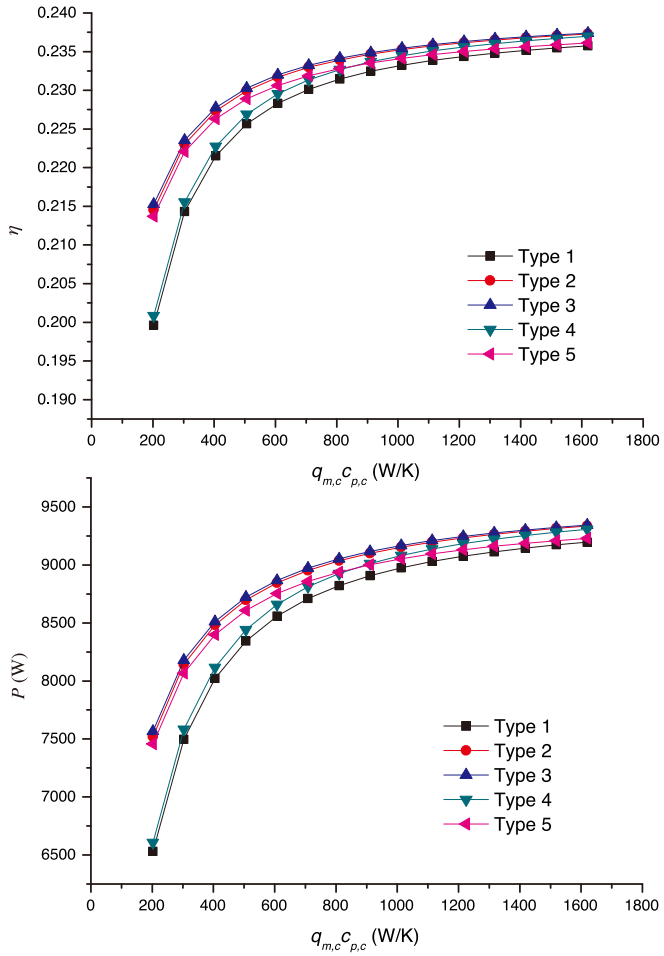


**Fig. 7.** Influence of $q_{m,c}c_{p,c}$ on efficiency and power of SEA.

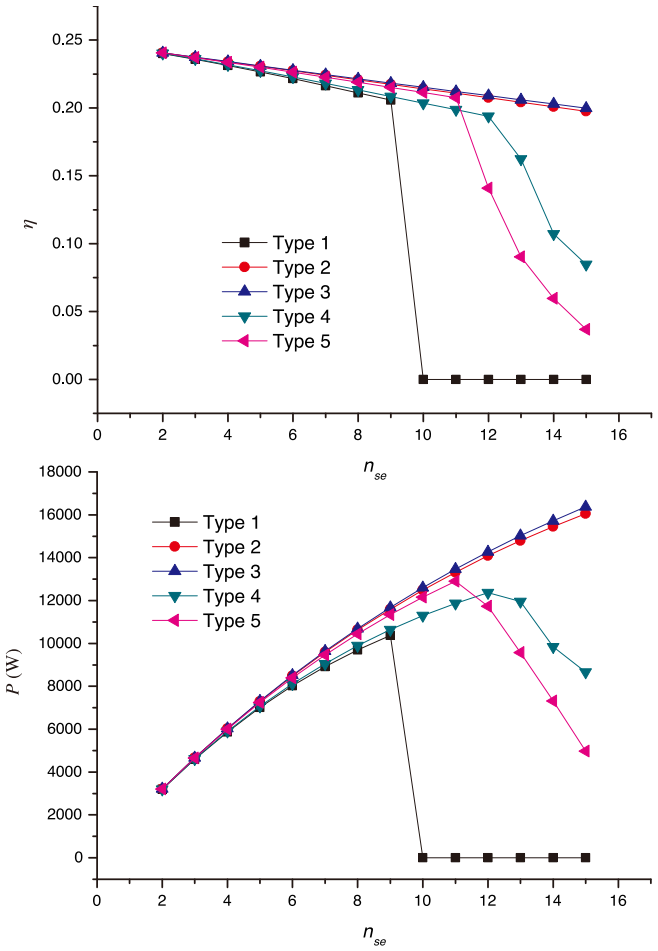


**Fig. 8.** Influence of $n_{se}$ on efficiency and power of SEA.

The flow order, co-current flow or counter-current flow, has little influence on the engine array performance. The difference of thermal efficiency of the SEA with Type 2 and Type 3 is from 0.04% to 0.39%; the difference of output power of the SEA with Type 2 and Type 3 is from 0.09% to 0.70%.

### 5.3. Effects of $n_{se}$

By varying the number of engines in SEA, the performance levels changed accordingly. $n_{se}$ may affects both the flow rates and temperatures of fluids of each engine. Fig. 8 shows curves of performance of SEAs with different $n_{se}$. As it is shown, with an increase of $n_{se}$ leads to a reduction of $\eta$ for all SEAs due to the decreasing of heating and cooling average temperature difference with increasing the number of engines. For some types of SEA, when $n_{se}$ is larger than a critical value, some of the engines in the SEA will not work and the curves will dive. E.g., for SEA of Type 1, when $n_{se}$ is larger than 9, all the engines stop working, turning points at 9 can be found on the $\eta$-$n_{se}$, $P$-$n_{se}$ curves in Fig. 8.

For Type 1, when $n_{se} > 9$, all engines stop working for given heating and cooling fluids due to small $q_m c_p$. For Type 2 and Type 3, every engine in the SEAs works, by increasing $n_{se}$, $\eta$ reduces due to a smaller temperature difference of the fluids, and $P$ increases due to more operating engines. For Type 4, by checking results, it can be found that when $n_{se} = 13$, the last engine does not work; when $n_{se} = 14$, only the first 10 engines will work; when $n_{se} = 15$, the working engine number drops to 9. For Type 5, by checking results, it can be found that when $n_{se} = 12$, the last 2 engines stop working; when $n_{se} = 13$, only the first 8 engines will work; when $n_{se} = 14$, the working engine number drops to 6; when $n_{se} = 15$, the working engine number drops to 4. This may be interpreted by the fact that the fluid flow rate $q_m$ in a parallel flow connection (Type 1, Type 4 and Type 5) is smaller and the temperature difference between the hot and cold fluid of the engine drops faster, resulting in a smaller number of engines that can work.

The flow order, co-current flow or counter-current flow, has little influence on the engine array performance. The difference of thermal efficiency of the SEA with Type 2 and Type 3 is from 0.02% to 1.19%; the difference of output power of the SEA with Type 2 and Type 3 is from 0.03% to 2.00%.

For a certain connection type, increase $n_{se}$ will reduce the efficiency of the SEA. For some connection types, increase $n_{se}$ will reduce the output power $P$ due to inoperative engines and smaller output power engines. It is important to choose the number of engines for some connection types of SEA.

## 6. Conclusions

A new layout scheme of the solar dish system by using SEA was proposed in this paper. The connection type of the engines may change the flow rates and temperatures of the fluids, as a result, the performance of the SEA will be different depending on the connection schemes. In order to compare the performance of SEAs with different arrangements, five basic connection types of SEA were summed up according to flow type and flow order.

An analytical Stirling engine model was created to develop the SEA models for the investigation of the influence of connection types. Imperfect regeneration and cycle irreversibility of Stirling engine cycle and heat exchange process between fluids and the engine were considered in the model. An algorithm to numerically solve different connection types of SEA was developed. The model was evaluated by considering the prototype GPU-3 Stirling engine as a case study. The result shows that the proposed model predicted the performance with higher accuracy than the Simple model (Urieli and Berchowitz, 1984) and Simple II model (Babaelahi and Sayyaadi, 2014). The proposed model improved errors ($s_{se} = 25$ Hz, $p = 4.14$ MPa) on the thermal efficiency and output power and reduced these errors from 7.49% and 110.11% (as difference) obtained in simple II model (Babaelahi and Sayyaadi, 2014) to 2.49% and 1.56% (as difference), respectively.

Models of SEAs were developed to calculated the performance under different parameters to find out the impacts of $T_{i,h}$, $q_{m,h}c_{p,h}$, $q_{m,c}c_{p,c}$ and $n_{se}$ on different connection types. It was found that, as expected, decrease $T_{i,h}$ and $q_m c_p$ will weaken the performance of SEA of all connection types. However, for some connection types, there exists a critical temperature below which some engines stop working. This needs to be considered for SEA connection type selection, especially when $T_{i,h}$ is low. For given heating and cooling fluids, Type 2 has the best performance and adaptability. Type 2 and Type 3 have similar performance under different parameters ($T_{i,h}$, $T_{i,c}$ and $q_m c_p$), which means the flow order has little influence (the maximum difference between thermal efficiency and output power is 0.39% and 0.70% respectively) on the performance of an SEA. SEA of serial flows (Type 3) has the best performance and adaptability under different parameters. Given heating and cooling fluids, using serial flow is the best choice for the connection type of an SEA.

It is important to note that, in future researches, the experiments of influence of connection type on SEA's performance can be carried out to verify the conclusions in this paper.

## CRediT authorship contribution statement

**Cheng Zhang:** Conceptualization, Writing - original draft, Read and contributed to the manuscript. **Qing Xu:** Investigation, Read and contributed to the manuscript. **Yanping Zhang:** Supervision, Read and contributed to the manuscript. **Inmaculada Arauzo:** Writing - review & editing, Supervision, Read and contributed to the manuscript. **Chongzhe Zou:** Data processing, Read and contributed to the manuscript.

## Declaration of competing interest

The authors declare that they have no known competing financial interests or personal relationships that could have appeared to influence the work reported in this paper.

## Acknowledgments

We gratefully acknowledge the support of the Project of Enhancing School with Innovation of Guangdong Ocean University (No. 230419098) and Joint Fund Project of Basic and Applied Basic Research Fund of Guangdong Province (No. 2019A1515111066), without which the present study could not have been completed.

## References

Abbas, M., 2014. Thermal analysis of Stirling engine solar driven. Cder Dz 70, 503–514.

Ahmadi, M.H., Ahmadi, M.A., Mellit, A., Pourfayaz, F., Feidt, M., 2016a. Thermodynamic analysis and multi objective optimization of performance of solar dish Stirling engine by the centrality of entransy and entropy generation. Int. J. Electr. Power Energy Syst. 78, 88–95.

Ahmadi, M.H., Ahmadi, M.A., Pourfayaz, F., Bidi, M., Hosseinzade, H., Feidt, M., 2016b. Optimization of powered Stirling heat engine with finite speed thermodynamics. Energy Convers. Manag. 108, 96–105.

Aichmayer, L., Spelling, J., Laumert, B., 2015. Preliminary design and analysis of a novel solar receiver for a micro gas-turbine based solar dish system. Sol. Energy 114, 378–396.

Araoz, J.A., Salomon, M., Alejo, L., Fransson, T.H., 2015. Numerical simulation for the design analysis of kinematic Stirling engines. Appl. Energy 159, 633–650. http://dx.doi.org/10.1016/j.apenergy.2015.09.024.

Babaelahi, M., Sayyaadi, H., 2014. Simple-ii: A new numerical thermal model for predicting thermal performance of stirling engines. Energy 69, 873–890.

Babaelahi, M., Sayyaadi, H., 2015. A new thermal model based on polytropic numerical simulation of Stirling engines. Appl. Energy 141, 143–159. http://dx.doi.org/10.1016/j.apenergy.2014.12.033.

Barreto, G., Canhoto, P., 2017. Modelling of a Stirling engine with parabolic dish for thermal to electric conversion of solar energy. Energy Convers. Manag. 132, 119–135.

Buscemi, A., Brano, V. Lo, Chiaruzzi, C., Ciulla, G., Kalogeri, C., 2020. A validated energy model of a solar dish-stirling system considering the cleanliness of mirrors. Appl. Energy 260, 114378. http://dx.doi.org/10.1016/j.apenergy.2019.114378.

Chen, L., Zhang, W., Sun, F., 2007. Power, efficiency, entropy-generation rate and ecological optimization for a class of generalized irreversible universal heat-engine cycles. Appl. Energy 84, 512–525.

Craig, K.J., Marsberg, J., Meyer, J.P., 2016. Combining ray tracing and CFD in the thermal analysis of a parabolic dish tubular cavity receiver. AIP Conf. Proc. 1734.

Duan, C., Wang, X., Shu, S., Jing, C., Chang, H., 2014. Thermodynamic design of Stirling engine using multi-objective particle swarm optimization algorithm. Energy Convers. Manag. 84, 88–96. http://dx.doi.org/10.1016/j.enconman.2014.04.003.

Formosa, F., Despesse, G., 2010. Analytical model for Stirling cycle machine design. Energy Convers. Manag. 51, 1855–1863. http://dx.doi.org/10.1016/j.enconman.2010.02.010.

Heywood, JohnB, 1988. Internal Combustion Engine Fundamentals. McGraw-Hill.

Hooshang, M., Moghadam, R.A., Alizadehnia, S., 2016. Dynamic response simulation and experiment for gamma-type Stirling engine. Renew Energy 86, 192–205. http://dx.doi.org/10.1016/j.renene.2015.08.018.

Hosseinzade, H., Sayyaadi, H., Babaelahi, M., 2015. A new closed-form analytical thermal model for simulating Stirling engines based on polytropic-finite speed thermodynamics. Energy Convers. Manag. 90, 395–408. http://dx.doi.org/10.1016/j.enconman.2014.11.043.

Jia, B., Smallbone, A., Feng, H., Tian, G., Zuo, Z., Roskilly, A.P., 2016. A fast response free-piston engine generator numerical model for control applications. Appl. Energy 162, 321–329.

Karabulut, H., Okur, M., Halis, S., Altin, M., 2019. Thermodynamic, dynamic and flow friction analysis of a Stirling engine with Scotch yoke piston driving mechanism. Energy 168, 169–181. http://dx.doi.org/10.1016/j.energy.2018.11.078.

Li, R., Grosu, L., Queiros-Conde, D., 2016. Multi-objective optimization of Stirling engine using Finite Physical Dimensions Thermodynamics (FPDT) method. Energy Convers. Manag. 124, 517–527.

Loni, R., Kasaeian, A.B., Asli-Ardeh, E.A., Ghobadian, B., Roux, W.G. Le, 2016. Performance study of a solar-assisted organic Rankine cycle using a dish-mounted rectangular-cavity tubular solar receiver. Appl. Therm. Eng. 108, 1298–1309.

Lovegrove, K., Luzzi, A., Soldiani, I., Kreetz, H., 2004. Developing ammonia based thermochemical energy storage for dish power plants. Sol. Energy 76, 331–337.

Luo, Z., Sultan, U., Ni, M., Peng, H., Shi, B., Xiao, G., 2016. Multi-objective optimization for GPU3 Stirling engine by combining multi-objective algorithms. Renew. Energy 94, 114–125. http://dx.doi.org/10.1016/j.renene.2016.03.008.

Martini, W.R., 1983. Stirling Engine Design Manual, second ed.

Ni, M., Shi, B., Xiao, G., Peng, H., Sultan, U., Wang, S., et al., 2016. Improved Simple Analytical Model and experimental study of a 100 W beta-type Stirling engine. Appl. Energy 169, 768–787.

Organ, A.J., 1997. The Regenerator and the Stirling Engine. Mech Eng Publ Ltd.

Patel, V., Savsani, V., 2016. Multi-objective optimization of a Stirling heat engine using TS-TLBO (tutorial training and self learning inspired teaching-learning based optimization) algorithm. Energy 95, 528–541.

Timoumi, Y., Tlili, I., Nasrallah, S. Ben, 2008. Design and performance optimization of GPU-3 Stirling engines. Energy 33, 1100–1114.

Urieli, I., Berchowitz, D.M., 1984. Stirling Cycle Engine Analysis. A. Hilger, Bristol.

Wang, W., Xu, H., Laumert, B., Strand, T., 2014. An inverse design method for a cavity receiver used in solar dish Brayton system. Sol. Energy 110, 745–755.

Wu, F., Chen, L., Wu, C., Sun, F., 1998. Optimum performance of irreversible Stirling engine with imperfect regeneration. Energy Convers. Manag. 39, 727–732.

Yaqi, L., Yaling, H., Weiwei, W., 2011. Optimization of solar-powered Stirling heat engine with finite-time thermodynamics. Renew. Energy 36, 421–427.